

Article

Excess Sludge Disintegration by Discharge Plasma Coupled with Thiosulfate

Hekai Jin ^{1,†} , Song Lin ^{2,†}, Yueyun Yang ¹, Zhixin Liang ¹, Yiqi Chen ¹, Lei Hua ¹, Ying Zhang ³, Hongtao Jia ⁴, Guodong Zhang ^{1,*} and Tiecheng Wang ^{1,*}

¹ College of Natural Resources and Environment, Northwest A&F University, Yangling 712100, China; jinhekai2002@163.com (H.J.); 18366137982@163.com (Y.Y.); zhixingliang@nwafu.edu.cn (Z.L.); yiqichen@nwafu.edu.cn (Y.C.); 13359481360@163.com (L.H.)

² College of Humanities and Law, Wuchang University of Technology, Wuhan 430223, China; linsongchina@126.com

³ College of Information Science and Technology, Nanjing Forestry University, Nanjing 210037, China; zhangying343@126.com

⁴ College of Resources and Environment, Xinjiang Agricultural University, Urumqi 830052, China; jht@xjau.edu.cn

* Correspondence: zhangguodong@nwafu.edu.cn (G.Z.); wangtiecheng2008@126.com (T.W.)

† These authors contributed equally to this work.

Abstract: Surplus sludge disposal and treatment are major issues in wastewater treatment plants. Discharge plasma oxidation is an effective approach for sludge dewatering and digestion. In this study, excess sludge disintegration by non-thermal discharge plasma coupled with thiosulfate (TSA) was investigated. After 20 min of the single discharge plasma treatment, the soluble chemical oxygen demand (SCOD) increased to 404.93 mg L⁻¹, and it climbed even more to 549.08 mg L⁻¹ after adding 15 mmol L⁻¹ of TSA. The water content of the filter cake also reduced even more in the presence of TSA. There was an appropriate dosage of TSA available. In the discharge plasma coupled with TSA system, reactive oxygen species ($\cdot\text{OH}$ and O_2^-) were generated and had significant involvement in the disintegration of the sludge. The addition of TSA enhanced the production of OH. These reactive oxygen species decomposed the floc structures and facilitated the transformation of organic compounds, resulting in a decrease in the average size of the sludge aggregates. The ratio of soluble extracellular polymer substances (S-EPS) was enhanced, while the ratio of the tightly bound fraction was reduced after the treatment. Thus, discharge plasma coupled with TSA promoted microbial cell lysis and facilitated the release of intracellular organic matter and bound water, ultimately enhancing the sludge's dewaterability.

Keywords: excess sludge; discharge plasma; thiosulfate; disintegration



Citation: Jin, H.; Lin, S.; Yang, Y.; Liang, Z.; Chen, Y.; Hua, L.; Zhang, Y.; Jia, H.; Zhang, G.; Wang, T. Excess Sludge Disintegration by Discharge Plasma Coupled with Thiosulfate.

Water **2023**, *15*, 3313. <https://doi.org/10.3390/w15183313>

Received: 14 August 2023

Revised: 16 September 2023

Accepted: 18 September 2023

Published: 20 September 2023



Copyright: © 2023 by the authors. Licensee MDPI, Basel, Switzerland. This article is an open access article distributed under the terms and conditions of the Creative Commons Attribution (CC BY) license (<https://creativecommons.org/licenses/by/4.0/>).

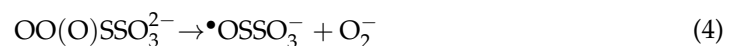
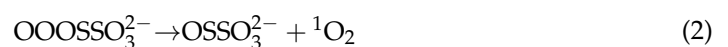
1. Introduction

The development of human civilization contributes to the generation of an increasing amount of domestic sewage and industrial wastewater, which enter wastewater treatment plants (WWTPs) [1]. Over 90% of municipal wastewater undergoes activated sludge biological treatment, resulting in substantial amounts of excess sludge caused by the rapid growth of microorganisms. This excessive sludge comprises numerous toxic and harmful substances, including parasites, viruses, pathogenic bacteria, heavy metal ions, and organic matter that is challenging to degrade. This poses a considerable threat to both the environment and human health [2]. In 2019, China produced over 36 million tons of sewage sludge with a moisture content of approximately 80%. How to dispose of this hazardous sludge in a cost-effective, non-secondary pollution-causing and recyclable manner has gained worldwide attention [3]. The high moisture content and poor dewatering performance of sewage sludge are well-known obstacles that significantly increase the operating costs of WWTPs. Sewage sludge contains both free and bound water [4]. The bound water, particularly that

bound to sewage sludge components such as flocculants, including extracellular polymers (EPS) [5], is highly challenging to remove.

Numerous techniques for sewage sludge treatment have been developed, including mechanical [6] and thermal treatment [7,8], chemical methods [9,10], microbiological treatment [11], ultrasound treatment [12], and microwave treatment [13]. These methods are capable of effectively achieving sewage sludge dewatering, although they also present certain limitations, including extended processing times, elevated costs, and limited utilization rates. With increasing volumes of sewage sludge, there arises a need for more efficient and expedited treatment methods. Advanced oxidation processes can produce strong oxidizing species (such as OH, O₂⁻, and SO₄⁻), which can effectively crack the sewage sludge cells and achieve dehydration [14–17]. Non-thermal discharge plasma has gained significant interest due to its high efficiency, simple equipment, and environmental friendliness [18,19]. Non-thermal discharge plasma has been widely used in the prevention and control of gaseous pollutants [20], water pollution treatment [15], sterilization, and disinfection [21]. Ozone is one of the main species produced in the non-thermal discharge plasma process [22,23], which has been reported to improve the dewaterability of sewage sludge [24]; however, the ozone produced by non-thermal discharge plasma is released into the atmosphere through aeration [23]. Moreover, ozone is less effective in removing difficult-to-degrade pollutants, such as endotoxins, while ozone oxidizes organic matter incompletely and the intermediates generated by decomposition may prevent further oxidation by ozone [24,25]. The aforementioned drawbacks diminish the efficiency of the non-thermal discharge plasma treatment applied to sewage sludge. Consequently, it is crucial to enhance the utilization of ozone in the non-thermal discharge plasma process.

Certain reducing agents are commonly utilized to catalyze the decomposition of ozone. Compared to nitrogen-containing reducing agents, sulfur-containing reducing agents do not generate toxic byproducts such as N-nitrosodimethylamine (NDMA) [25]. In ozone systems, thiosulfate is frequently employed as an ozone terminator [26,27]. When the thiosulfate concentration (TSA) is low, it can facilitate the generation of free radicals by ozone. The ensuing reactions (Equations (1)–(10)) are presented below [28,29]. Low concentrations of TSA enhance ozone oxidation for the purpose of desulfurization and denitrification [28]. Yang et al. [29] found that adding TSA at relatively low concentrations during the ozonation process significantly enhances the oxidation of refractory contaminants. There is currently insufficient information on the potential of TSA to promote the dewatering of sewage sludge in the non-thermal discharge plasma process.



In this study, the utilization of non-thermal discharge plasma coupled with thiosulfate for the disintegration of excess sludge was examined. The primary goals of this study were as follows: (1) to assess the impact of non-thermal discharge plasma combined with thiosulfate on the dewatering of sewage sludge, (2) to investigate the sewage sludge dewatering process, and (3) to unveil the reaction mechanisms of non-thermal discharge plasma combined with thiosulfate in sewage sludge dewatering.

2. Materials and Methods

2.1. Sludge Collection and Chemicals

All the sludge used in this study was collected daily from the active sludge return unit of a wastewater treatment plant (WWTP) utilizing an anaerobic–anoxic–oxic process with a treatment capacity of 40,000 m³ per day. The WWTP is situated in Yangling, Shaanxi, China, specifically at coordinates 108°4′27.95″ E and 34°16′56.24″ N. The sewage sludge was promptly transferred to the laboratory and stored in a refrigerator at a temperature of 4 °C. Prior to conducting the experiments, the sewage sludge was thoroughly shaken and allowed to reach room temperature. Sodium thiosulfate (Na₂S₂O₃) was purchased from Kermel Chemical Reagent Co., Ltd. (Tianjin, China). Terephthalic acid (C₈H₆O₄) and *p*-benzoquinone (C₆H₄O₂) were purchased from Shanghai Macklin Biochemical Co., Ltd. (Shanghai, China). Potassium dichromate (K₂Cr₂O₇), silver sulfate (Ag₂SO₄), sulfuric acid (H₂SO₄), sodium hydroxide (NaOH), sodium chloride (NaCl), copper sulfate (CuSO₄), isopropanol (C₃H₈O), and phenol (C₆H₅OH) were purchased from Kermel Chemical Reagent Co., Ltd. (Tianjin, China). Foline-phenol was purchased from Beijing Solarbio Science & Technology Co., Ltd. (Beijing, China). All the chemicals were of analytical grade and were used without further purification.

2.2. Experimental Section

The system for the sewage sludge disintegration comprised three main components: the discharge plasma system, the reverse-flow system, and the reactor, as illustrated in Figure 1. In the discharge plasma system, the discharge electrode was a stainless-steel wire with a pitch of 0.8 cm and a length of 10 cm. This wire was tightly inserted into a quartz-glass tube measuring 1 cm in inner diameter, 1 mm in wall thickness, and 15 cm in length. The quartz-glass tube was used as the discharge barrier. The ground electrode was composed of sewage sludge with an inserted wire. Natural air served as the carrier gas after passing through a column of color-changing silica gel to eliminate any water molecules. Dry air served as the gas source for the generation of the reactive oxygen species (ROS). The ROS were injected into the quartz-glass tube in the form of small bubbles with a flow rate of 120 L h⁻¹. An AC-stabilized power source (CTP-2000K) was used, which was purchased from Nanjing Suman Electronics Co., Ltd. (Nanjing, China). The discharge voltage was 3 kV and the discharge frequency was 7 kHz in this study. The reactor used for the sewage sludge disintegration was a plexiglass tube, which had an inner diameter of 4 cm, a wall thickness of 2 mm, and a length of 25 cm. The following procedures were implemented to trigger the discharge plasma. Initially, dry air was injected into the quartz-glass tube. Subsequently, the quartz-glass tube was placed into the untreated sewage sludge. Finally, a specific voltage was applied to the electrodes to initiate the discharge plasma. The plasma would be generated in the gas phase along the quartz-glass tube wall (internal section of the reactor) under the action of airflow, and then the generated ROS (such as ·OH, ·O₂⁻, and O₃) would be injected into the sewage sludge (external section of the reactor) in the form of bubbles through an aerator at the bottom of the quartz-glass tube. For each batch experiment, a total of 300 mL of the raw sludge suspension containing varying concentrations of TSA was mixed and subsequently introduced into the discharge reactor. The sewage sludge suspension was circulated during the treatment using a peristaltic pump. All the experiments were conducted in triplicate.

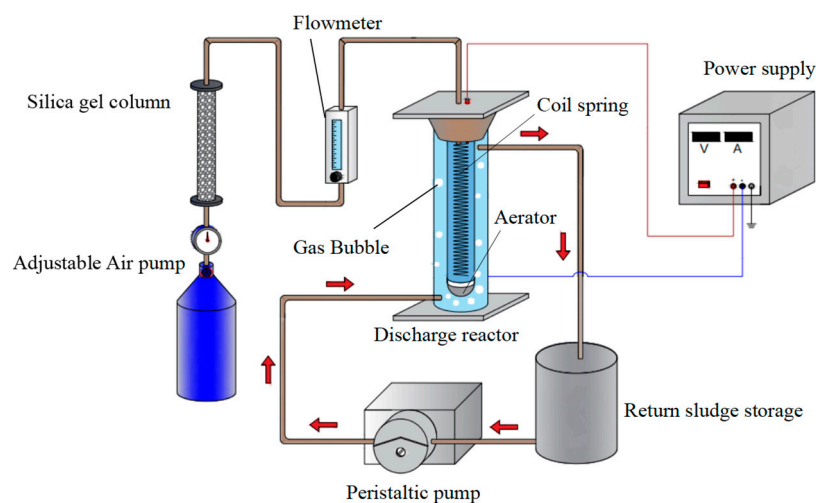


Figure 1. Schematic diagram of the sewage sludge disintegration system.

2.3. Analytical Methods

A laser diffraction particle size analyzer (Mastersizer APA 2000, Malvern Instruments Ltd., Malvern, UK) was used to determine the particle size distribution of the flocs. The sewage sludge obtained from various treatments underwent centrifugation at 3000 rpm for 10 min, resulting in the separation of the supernatant. The sewage sludge was freeze-dried and sputtered with gold prior to analysis using scanning electron microscopy (SEM; Hitachi S-4800, Tokyo, Japan). The sewage sludge suspension underwent centrifugation in a 50 mL centrifuge tube at $3000\times g$ for 10 min, and the supernatant was collected as soluble EPS (S-EPS). A heat extraction method was used to extract the loosely bound EPS (LB-EPS) and tightly bound EPS (TB-EPS) [30]. In more detail, the suspension of sewage sludge was centrifuged in a 50 mL centrifuge tube at $3000\times g$ for 10 min. The resulting supernatant was collected as soluble extracellular polymeric substances (S-EPS). The remaining sewage sludge in the tube was subsequently resuspended in 15 mL of a 0.05% NaCl solution. This resuspended sludge was then subjected to sonication at 20 kHz for 2 min, followed by horizontal shaking at 150 rpm for 10 min, and then another round of sonication for 2 min. Afterward, the suspension was centrifuged at $8000\times g$ for 10 min to separate the components, with the resulting supernatant being considered loosely bound EPS (LB-EPS). The remaining sewage sludge pellet in the tube was then resuspended in a 0.05% NaCl solution, subjected to 3 min of sonication, shaken for 10 min, and sonicated again for 3 min. Following this, the suspension was heated at 60 °C in a water bath for 30 min and finally centrifuged at $12,000\times g$ for 20 min. The resulting liquid was collected as tightly bound EPS (TB-EPS). Before analysis, all the fractions were filtered through a 0.45 μm filter membrane to eliminate any particulate matter.

The dissolved organic carbon (DOC) in the EPS was detected using a total organic carbon analyzer (TOC MultiN/CUV, Analytic Jena, Jena, Germany). The polysaccharides (PS) in the EPS were quantified via the phenol–sulfuric acid process [31]. The protein (PN) content of the EPS was measured using the modified Lowry method [32]. The three-dimensional fluorescence spectra (3D-EEM) of the different EPS fractions were obtained using a fluorescence spectrometer (F-4600, Hitachi, Japan), and the constituent substances were then analyzed using parallel factor analysis (PARAFAC). The PARAFAC analysis was conducted using the DOM Fluor v.1.7 toolbox in the MATLAB R2018a software (MathWorks, Carlsbad, CA, USA). Additionally, outliers were eliminated via Rayleigh scattering and Raman scattering tests. In more detail, the samples were filtered through a 0.45 μm cellulose membrane prior to measurement. EEM scans were performed at emission wavelengths (E_m) ranging from 200 to 400 nm, with 5 nm increments, and excitation wavelengths (E_x) ranging from 200 to 400 nm, with a step size of 5 nm. The bandwidths of both the E_x/E_m slits were set to 5 nm. Split-half analysis and residual analysis were then used to assess the

viability of the parallel factor model. Finally, several iterations were used to establish the DOM components. The Fourier transform infrared (FT-IR) spectroscopy analysis of the EPS was conducted using a Vetex 70 Fourier infrared spectrometer instrument manufactured by Bruck in Brandenburg, Germany. The analysis of the fluorescence intensity was performed using a Hitachi F-4600 fluorescence spectrometer.

The soluble chemical oxygen demand (SCOD), the settling velocity (SV_{30}), and the sludge moisture content of the filter cake ($Wc\%$) of the sewage sludge were detected via the determination of the chemical oxygen demand, fast digestion-spectrophotometric analysis (HJ/T 399-2007), the sludge settling ratio (CJ/T 221-2005), and the gravimetric method (and CJ/T 221-2005) [33]. Additionally, the calculation of dewaterability was performed as described below.

The dewaterability was calculated as follows:

$$\text{Dewaterability} = \frac{m_{\text{wet}} - m_{\text{dry}}}{m_{\text{wet}}} \quad (11)$$

where m_{wet} and m_{dry} represent the wet and dry weights of the mud, respectively.

3. Results and Discussion

3.1. Sewage Sludge Disintegration Performance

During the oxidation process, the microbial cells in the sludge are disrupted and the intracellular and pericellular EPS components, such as proteins and polysaccharides, are released into the water, which in turn leads to an increase in the SCOD [34]. Therefore, changes in the SCOD of the sewage sludge can be utilized to assess the efficacy of sewage sludge disintegration [34]. Figure 2a illustrates that at low TSA concentrations (0 mmol L^{-1} , 1 mmol L^{-1} , and 5 mmol L^{-1}), the SCOD increased with an increase in the treatment time. When the TSA concentration reached high levels ($10\text{--}20 \text{ mmol L}^{-1}$), the SCOD exhibited a decrease. Moreover, Figure 2b demonstrates that the concentration of thiosulfate at various concentrations ranging from 1 to 20 mmol L^{-1} contributed 19% to 77% of the SCOD. Meanwhile, the moisture content of the filter cake initially decreased and subsequently increased with the TSA dosage (Figure 2c). The moisture content of the filter cake was the lowest when the concentration of TSA was 15 mmol L^{-1} , which supported the findings of the SCOD analysis. Therefore, the results concerning the SCOD and moisture content indicated that the optimum level of TSA in this system was 15 mmol L^{-1} . At low concentrations of TSA, ozone can expedite the generation of free radicals, while high concentrations of TSA inhibit these reactions [28,29]. The SCOD generally increased after 20 min of processing with an increase in the TSA dosage. The SCOD concentration of the untreated sludge was 222.38 mg L^{-1} . The SCOD increased to 404.93 mg L^{-1} after 20 min of the single discharge plasma treatment, and it further increased to 549.08 mg L^{-1} after adding 15 mmol L^{-1} of TSA. In the presence of low concentrations of TSA, more amounts of free radicals would be generated, and the free radicals oxidized some organic matter in the sludge [34,35]. Additionally, the moisture content of the filter cake was 83.55% after 20 min of the discharge plasma treatment with the addition of 15 mmol L^{-1} of TSA. This phenomenon could be attributed to the fact that the strong oxidizing free radicals generated by the discharge plasma destroyed the microbial cells and block floc structures in the sludge, which resulted in a reduction in the moisture content [29,36]. These results also demonstrated that TSA was beneficial in improving the sludge dewatering in the discharge plasma process.

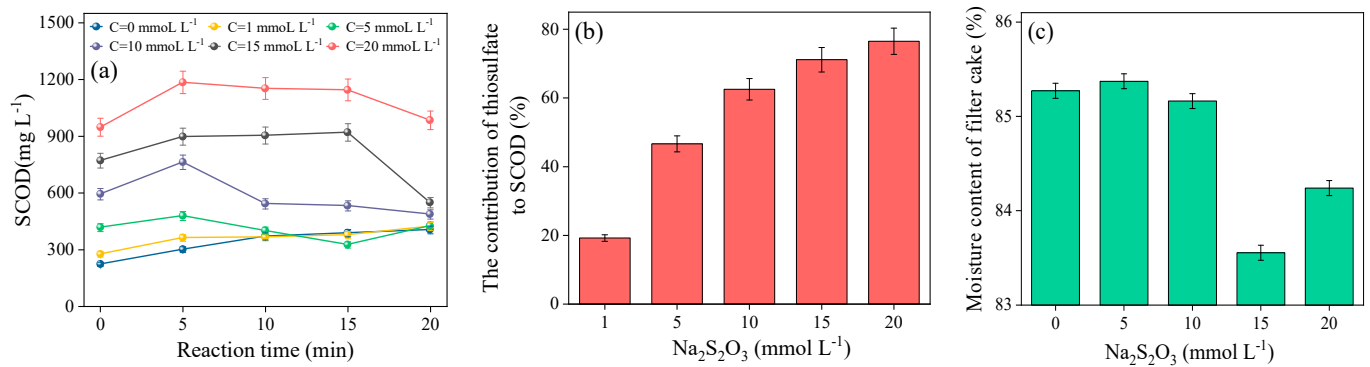


Figure 2. (a) Changes in the SCOD with the reaction time under different dosages of thiosulfate; (b) contributions of different concentrations of thiosulfate; and (c) moisture content of the filter cake.

3.2. Changes in the Sludge Particle Size and Morphology during the Dewatering Process

Changes in the sludge morphology can be used to characterize the dewatering process of sludge via discharge plasma treatment. As shown in Figure 3, the surface of the initial sewage sludge without any treatment was compact and had a complete structure, making it difficult to dehydrate. After the discharge plasma treatment, the sludge floc became looser and finer, and the surface also became coarser, especially in the presence of TSA. The strong oxidizing free radicals generated by the discharge plasma system destroyed the microbial cells and massive floc structures, and they promoted the release of organic matter and water in the floc from the mud to the water phase [36]. On the other hand, the EPS wrapping on the surface of the floc was destroyed by the oxidation of the free radicals [37]. With the prolongation of the treatment time, the large sludge flocs were cracked into fragments with smaller particle sizes and more organic matter and water were released into the liquid phase. Moreover, these dispersed small sludge fragments did not reaggregate into large flocs. These changes in the sludge morphology indicated that the discharge plasma technology can permanently change the surface morphology and structures of sludge flocs, which was consistent with previous studies [36,38].

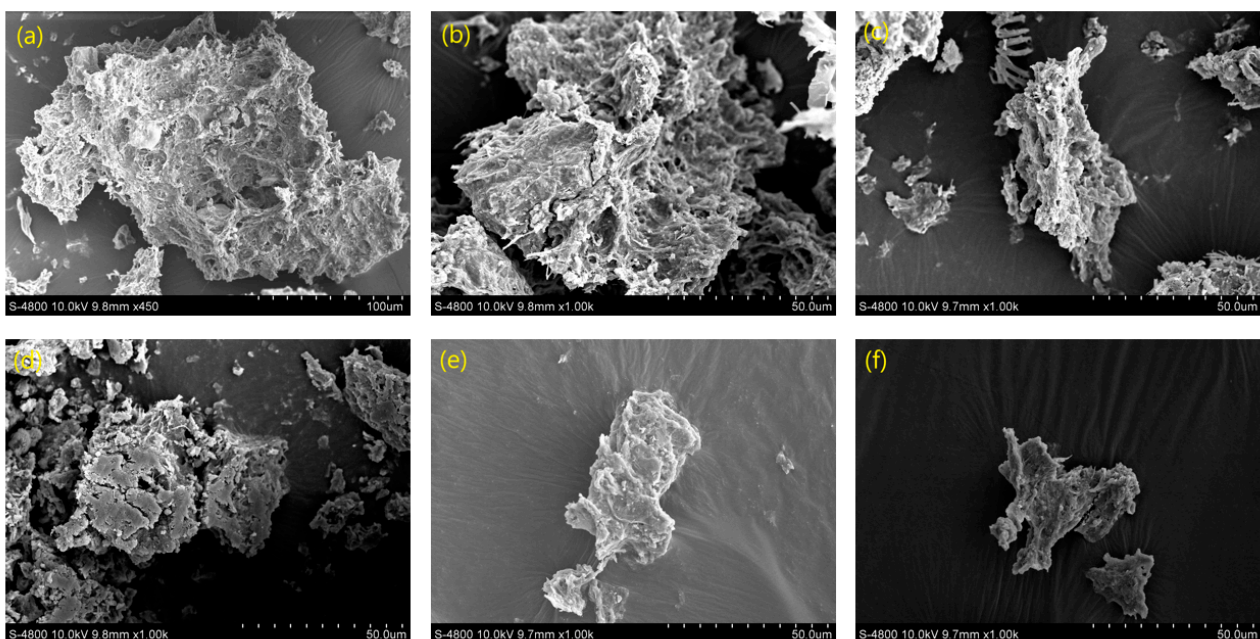


Figure 3. SEM of sludge ((a): raw sludge; (b): plasma treatment for 20 min; (c–f): discharge plasma coupled with TSA treatment for 5, 10, 15, and 20 min, respectively).

As shown in Figure 4a, the discharge plasma coupled with TSA treatment increased the proportion of small particles (0.01–0.5, 0.5–1, 1–2, 2–5, 5–10, and 10–20 μm) of sludge, and the proportion was much higher with the processing. However, the proportion of large particles (20–50, 50–100, 100–200, 200–250, 250–500, 500–1000, and >1000 μm) exhibited a gradually decreasing trend. This was consistent with the results concerning the sludge morphology. The changes in the average particle size and specific surface area of the sludge under various treatments are visible in Figure 5b. After 5, 10, 15, and 20 min of treatment, the average particle size of the sludge gradually decreased from the initial 49.8 μm to 37.9, 34.7, 26.3, and 25.5 μm, while the specific surface area gradually increased from 0.746 m² g⁻¹ to 0.978, 1.07, 1.41, and 1.46 m² g⁻¹, respectively. Similar results were also obtained during sludge cracking via the electro-Fenton technique [34,36]. These results suggested that the oxidizing species could destroy the structure and integrity of the sludge flocs.

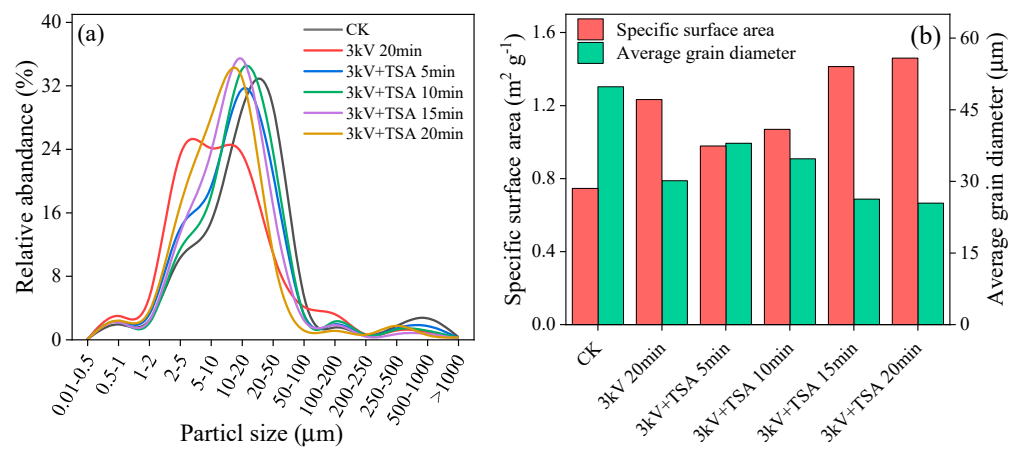


Figure 4. Evolution of the particle size distribution (a) and average size and specific surface area (b) of the sludge samples.

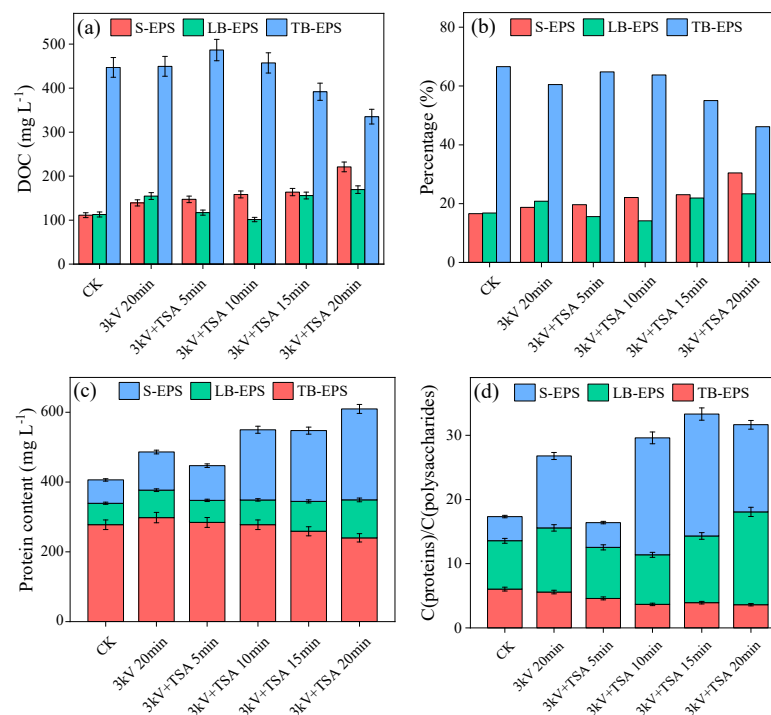


Figure 5. Evolution of the EPS distribution ((a): content; (b): percentage) and its composition ((c): proteins; (d): C(proteins)/C(polysaccharides)).

3.3. Changes in the EPS Distribution

EPS is an important component of sludge, accounting for 60–80% of the total weight of the sludge, and it can affect the physical and chemical properties of the sludge [3]. In addition to the occurrence of microbial cell lysis during sludge cracking, the transformation of EPS is also quite important. As illustrated in Figure 5a, the content of TB-EPS in the raw sludge (447.0 DOC mg L⁻¹) was much higher than that of SPES (111.3 DOC mg L⁻¹) and LB-EPS (112.8 DOC mg L⁻¹). After the discharge plasma and TSA treatment, the contents of S-EPS and LB-EPS exhibited increasing trends, while the content of TB-EPS decreased. As shown in Figure 5b, after 5, 10, 15, and 20 min of treatments, the proportion of TB-EPS gradually decreased from 66.6% to 64.8%, 63.8%, 55.1%, and 46.2%, respectively, and that of S-EPS also gradually increased from 16.6% to 19.6%, 22.1%, 23.0%, and 30.5%, respectively. This phenomenon was due to the continuous conversion of TB-EPS into S-EPS and LB-EPS during the sludge lysis process [39,40]. Proteins and polysaccharides are considered to be the two most important components of EPS, and the ratio of proteins to polysaccharides is considered an important indicator used to characterize the dewatering performance of sludge [41]. As shown in Figure 5c–d, the changes in the protein contents and the ratio of proteins to polysaccharides were consistent with the changes in the EPS. Since proteins and polysaccharides generally exist in the form of complexes in EPS, they generally exhibit the same pattern of changes [39]. Moreover, the free radicals generated in the discharge plasma system could directly destroy the free microbial cells or penetrate into the interior of the sludge floc, resulting in the release of intracellular organic matter (like proteins and polysaccharides), which was manifested by the increased EPS contents [42,43]. These results indicated that the discharge plasma and TSA treatment could affect the evolution of various types of EPS.

Furthermore, 3D-EEM is generally used to characterize the changes in the organic components of EPS [44,45]. The 3D-EEM spectra can be roughly divided into four zones, aromatic protein (I), fulvic acid-like zone (II), soluble microbial by-products (III), and humic acid-like zone (IV), with corresponding excitation/emission (EX/EM) wavelengths of 200–250/200–380 nm, 200–250/380–500 nm, 250–400/200–380 nm, and 250–400/380–500 nm, respectively [45]. As shown in Figures S1–S3, the 3D-EEM spectra of the EPS of the initial sludge exhibited two fluorescence peaks (A and B), and their specific locations (EX/EM) were roughly 280/330 nm (peak A) and 225/325 nm (peak B), corresponding to soluble microbial by-products and aromatic proteins, respectively [44,45]. Two main fluorescence components (C1 and C2) of the 3D-EEM spectra of the EPS were diagnosed, and their changes are shown in Figure 6. The C1 and C2 corresponded to the aromatic proteins and soluble microbial by-products, respectively. The changes in the fluorescence intensities of the C1 and C2 gradually increased in the S-EPS and LB-EPS. This could be due to the combined actions of the lysing of microbial cells (including free microorganisms in the water phase and encapsulated microorganisms in the mud), the transfer of organic components (from TB-EPS to S-EPS and LB-EPS), and the oxidative degradation of organic matter by the free radicals. During the first 5 min of treatment, the changes in the fluorescence intensities of the C1 and C2 gradually increased in the TB-EPS, while they gradually decreased within 10–20 min of treatment. These findings were mainly caused by the transfer of organic components in the TB-EPS, the lysis of microorganisms in the mud, and the oxidative degradation of organic matter [35]. Furthermore, the TB-EPS was initially (0–5 min) dominated by the lysis of microorganisms and the transfer of organic components, and then by the organic matter degradation. These findings were similar to those of previous studies [35,46].

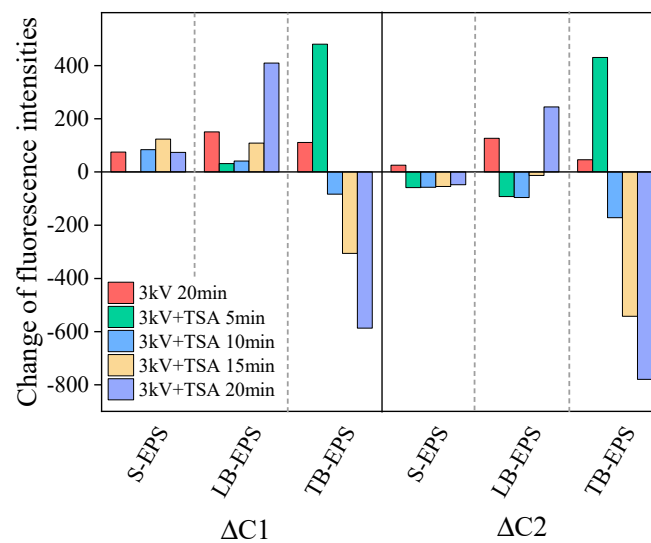


Figure 6. Changes in the fluorescence intensities of the C1 and C2 under different treatments compared to the raw sludge.

3.4. Mechanisms of Sludge Cracking

To analyze the mechanisms of sludge cracking in the discharge plasma coupled with TSA system, radical quenching experiments were conducted by adding trapping agents. Here, $\cdot\text{OH}$ and O_2^- can be quenched by isopropyl alcohol and *p*-benzoquinone, respectively [25]. As shown in Figure 7, with the increase in the *p*-benzoquinone concentration, the settling velocity (SV_{30}) of the sludge increased, and the contents of proteins and polysaccharides in the EPS showed obvious decreasing trends. The addition of isopropanol also resulted in similar effects, as shown in Figure 8. With increasing concentrations of the trapping agents, the number of free radicals involved in the sludge cracking became less, which made the settling and cracking performances of the sludge become worse. These results demonstrated that OH and O_2^- played important roles in the sludge cracking process. As shown in Figures 7 and 8, the influence of $\cdot\text{OH}$ on the EPS components was greater than that of $\cdot\text{O}_2^-$. Therefore, $\cdot\text{OH}$ played more important roles.

To further verify the roles of the free radicals, the $\cdot\text{OH}$ produced by the discharge plasma coupled with TSA system was analyzed via fluorescence analysis, and terephthalic acid (PTA) was used as an indicator of $\cdot\text{OH}$ [47,48]. According to previous studies, the characteristic peak of hydroxy-terephthalic acid (HTA) at 440 nm and the characteristic peak of the solvent at 314 nm could be observed [48]. As shown in Figure 9a, with the increase in the TSA concentration, the content of HTA produced by the reactions of PTA with $\cdot\text{OH}$ increased, which proved the roles of $\cdot\text{OH}$ in the system. To better study the relationship between $\cdot\text{OH}$ and TSA, a semi-quantitative analysis of the fluorescence intensity of HTA under different concentrations of TSA was conducted. As shown in Figure 9b, with the increase in the TSA concentration, the fluorescence intensity of HTA increased almost linearly. That is, the $\cdot\text{OH}$ produced by the discharge plasma system also increased linearly with the TSA addition. Previous studies also reported that a linear increase in the $\cdot\text{OH}$ concentration with an increasing thiosulfate concentration occurred in a thiosulfate-activated ozone system [29].

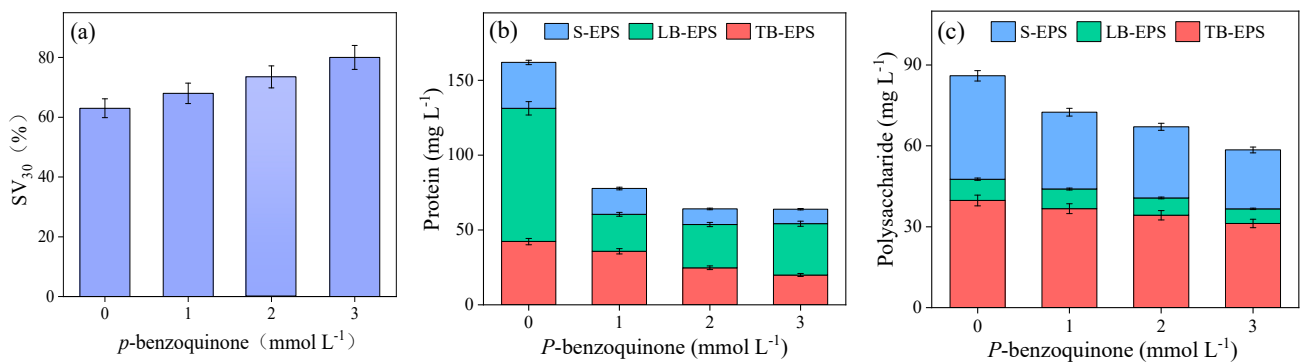


Figure 7. Effect of p-benzoquinone on the SV₃₀ (a), proteins (b), and polysaccharides (c) in the sludge.

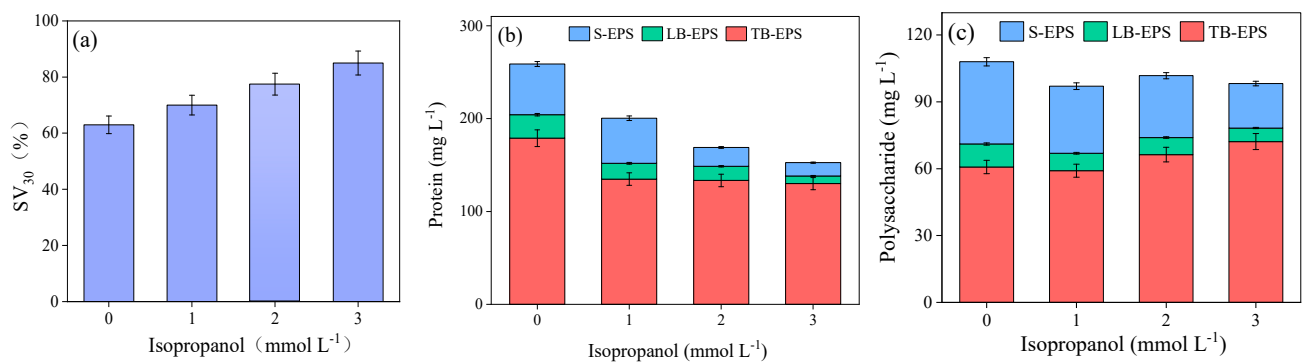


Figure 8. Effect of isopropanol on the SV₃₀ (a), proteins (b), and polysaccharides (c) in the sludge.

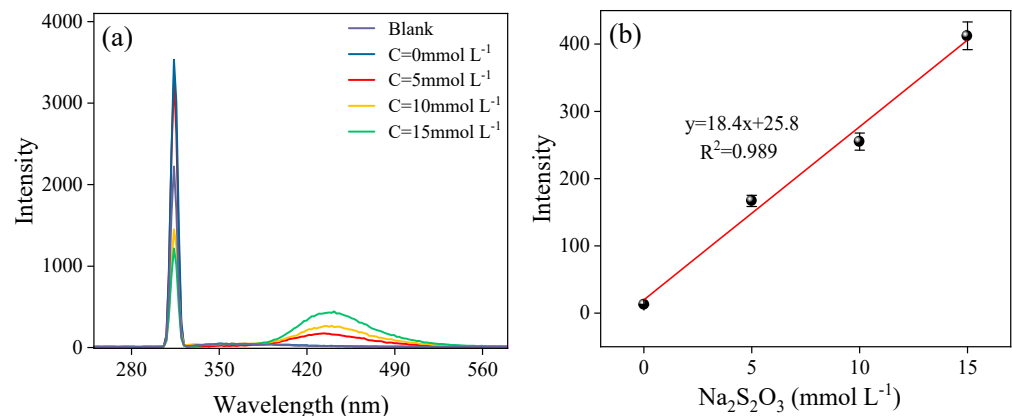


Figure 9. Fluorescence intensity of ·OH with the concentration of TSA (a) and the intensity of HTA as a function of TSA (b).

4. Conclusions

In this study, the effect of discharge plasma coupled with thiosulfate on sludge disintegration was evaluated. The discharge plasma oxidation coupled with thiosulfate promoted the sludge disintegration under different dosages of thiosulfate. During the treatment, reactive oxygen species ($\cdot\text{OH}$ and O_2^-) oxidation caused cell lysis and destructed the sludge flocs, which together induced the enhancement of the EPS contents and redistribution among various EPS fractions. Moreover, 3D-EEM and PARAFAC modeling analysis of the EPS demonstrated that the migration and decomposition of the EPS were the main processes behind the EPS changes. The intact and dense surface morphology of the sludge flocs was broken down into smaller fragments. Meanwhile, the intracellular bound water in the sludge flocs was released outside as free water.

Supplementary Materials: The following supporting information can be downloaded at: <https://www.mdpi.com/article/10.3390/w15183313/s1>, Figure S1: 3D-EEM of S-EPS (a: Raw sludge; b: plasma treatment for 20 min; c–f: discharge plasma coupled with TSA treatment for 5, 10, 15, and 20 min, respectively); Figure S2: 3D-EEM of LB-EPS (a: Raw sludge; b: plasma treatment for 20 min; c–f: discharge plasma coupled with TSA treatment for 5, 10, 15, and 20 min, respectively); Figure S3: 3D-EEM of TB-EPS (a: Raw sludge; b: plasma treatment for 20 min; c–f: discharge plasma coupled with TSA treatment for 5, 10, 15, and 20 min, respectively).

Author Contributions: Writing—original draft preparation, H.J. (Hekai Jin) and S.L.; investigation, Y.Y., Z.L., Y.C. and L.H.; methodology, Y.Z.; conceptualization, H.J. (Hongtao Jia); writing—review and editing, G.Z. and T.W.; project administration, T.W. All authors have read and agreed to the published version of the manuscript.

Funding: The authors thank the National Natural Science Foundation of China (42377388).

Institutional Review Board Statement: Not applicable.

Informed Consent Statement: Not applicable.

Data Availability Statement: Figures Data and Supplementary File Data were uploaded to figshare with doi:10.6084/m9.figshare.24161694.

Conflicts of Interest: The authors declare no conflict of interest.

References

1. Xu, Q.; Li, X.; Ding, R.; Wang, D.; Liu, Y.; Wang, Q.; Zhao, J.; Chen, F.; Zeng, G.; Yang, Q.; et al. Understanding and mitigating the toxicity of cadmium to the anaerobic fermentation of waste activated sludge. *Water Res.* **2017**, *124*, 269–279. [[CrossRef](#)] [[PubMed](#)]
2. Gutierrez, M.C.; Serrano, A.; Siles, J.A.; Chica, A.F.; Martin, M.A. Centralized management of sewage sludge and agro-industrial waste through co-composting. *J. Environ. Manag.* **2017**, *196*, 387–393. [[CrossRef](#)] [[PubMed](#)]
3. Chen, Z.; Zhang, W.; Wang, D.; Ma, T.; Bai, R. Enhancement of activated sludge dewatering performance by combined composite enzymatic lysis and chemical re-flocculation with inorganic coagulants: Kinetics of enzymatic reaction and re-flocculation morphology. *Water Res.* **2015**, *83*, 367–376. [[CrossRef](#)]
4. Zhen, G.; Lu, X.; Wang, B.; Zhao, Y.; Chai, X.; Niu, D.; Zhao, T. Enhanced dewatering characteristics of waste activated sludge with Fenton pretreatment: Effectiveness and statistical optimization. *Fron. Environ. Sci. Eng.* **2014**, *8*, 267–276. [[CrossRef](#)]
5. Neyens, E.; Baeyens, J.; Dewil, R.; De heyder, B. Advanced sludge treatment affects extracellular polymeric substances to improve activated sludge dewatering. *J. Hazard. Mater.* **2004**, *106*, 83–92. [[CrossRef](#)]
6. Zubrowska-Sudol, M.; Walczak, J. Enhancing combined biological nitrogen and phosphorus removal from wastewater by applying mechanically disintegrated excess sludge. *Water Res.* **2015**, *76*, 10–18. [[CrossRef](#)] [[PubMed](#)]
7. Feng, X.; Deng, J.; Lei, H.; Bai, T.; Fan, Q.; Li, Z. Dewaterability of waste activated sludge with ultrasound conditioning. *Bioresour. Technol.* **2009**, *100*, 1074–1081. [[CrossRef](#)]
8. Ye, F.; Liu, X.; Li, Y. Effects of potassium ferrate on extracellular polymeric substances (EPS) and physicochemical properties of excess activated sludge. *J. Hazard. Mater.* **2012**, *199*, 158–163. [[CrossRef](#)]
9. Cao, B.; Zhang, W.; Wang, Q.; Huang, Y.; Meng, C.; Wang, D. Wastewater sludge dewaterability enhancement using hydroxyl aluminum conditioning: Role of aluminum speciation. *Water Res.* **2016**, *105*, 615–624. [[CrossRef](#)]
10. Zahedi, S.; Icaran, P.; Yuan, Z.; Pijuan, M. Effect of free nitrous acid pre-treatment on primary sludge at low exposure times. *Bioresour. Technol.* **2017**, *228*, 272–278. [[CrossRef](#)]
11. Lu, Y.; Zhang, C.; Zheng, G.; Zhou, L. Improving the compression dewatering of sewage sludge through bioacidification conditioning driven by *Acidithiobacillus ferrooxidans*: Dewatering rate vs. dewatering extent. *Environ. Technol.* **2019**, *40*, 3176–3189. [[CrossRef](#)] [[PubMed](#)]
12. Ning, X.-A.; Chen, H.; Wu, J.; Wang, Y.; Liu, J.; Lin, M. Effects of ultrasound assisted Fenton treatment on textile dyeing sludge structure and dewaterability. *Chem. Eng. J.* **2014**, *242*, 102–108. [[CrossRef](#)]
13. Anjum, M.; Al-Talhi, H.A.; Mohamed, S.A.; Kumar, R.; Barakat, M.A. Visible light photocatalytic disintegration of waste activated sludge for enhancing biogas production. *J. Environ. Manag.* **2018**, *216*, 120–127. [[CrossRef](#)] [[PubMed](#)]
14. Feki, E.; Khoufi, S.; Loukil, S.; Sayadi, S. Improvement of anaerobic digestion of waste-activated sludge by using H₂O₂ oxidation, electrolysis, electro-oxidation and thermo-alkaline pretreatments. *Environ. Sci. Pollut. Res.* **2015**, *22*, 14717–14726. [[CrossRef](#)]
15. Shi, P.; Su, R.; Zhu, S.; Zhu, M.; Li, D.; Xu, S. Supported cobalt oxide on graphene oxide: Highly efficient catalysts for the removal of Orange II from water. *J. Hazard. Mater.* **2012**, *229*, 331–339. [[CrossRef](#)]
16. Yuan, H.-P.; Yan, X.-F.; Yang, C.-F.; Zhu, N.-W. Enhancement of waste activated sludge dewaterability by electro-chemical pretreatment. *J. Hazard. Mater.* **2011**, *187*, 82–88. [[CrossRef](#)]
17. Divyapriya, G.; Nambi, I.M.; Senthilnathan, J. An innate quinone functionalized electrochemically exfoliated graphene/Fe₃O₄ composite electrode for the continuous generation of reactive oxygen species. *Chem. Eng. J.* **2017**, *316*, 964–977. [[CrossRef](#)]

18. Ching, W.K.; Colussi, A.J.; Sun, H.J.; Nealon, K.H.; Hoffmann, M.R. Escherichia coli disinfection by electrohydraulic discharges. *Environ. Sci. Technol.* **2001**, *35*, 4139–4144. [[CrossRef](#)]
19. Ren, J.; Li, J.; Lv, L.; Wang, J. Degradation of caffeic acid by dielectric barrier discharge plasma combined with Ce doped CoOOH catalyst. *J. Hazard. Mater.* **2021**, *402*, 123772. [[CrossRef](#)]
20. Mok, Y.S.; Nam, C.M.; Cho, M.H.; Nam, I.S. Decomposition of volatile organic compounds and nitric oxide by nonthermal plasma discharge processes. *IEEE Trans. Plasma Sci.* **2002**, *30*, 408–416.
21. Larouss, M. The biomedical applications of plasma: A brief history of the development of a new field of research. *IEEE Trans. Plasma Sci.* **2008**, *36*, 1612–1614. [[CrossRef](#)]
22. He, Y.; Sang, W.; Lu, W.; Zhang, W.; Zhan, C.; Jia, D. Recent Advances of Emerging Organic Pollutants Degradation in Environment by Non-Thermal Plasma Technology: A Review. *Water* **2022**, *14*, 1351. [[CrossRef](#)]
23. Ye, Q.; Wan, H.; Lei, Y.; Zhang, J.; Li, J. Study on the technique of water-treatment by discharge plasma. *High Voltage Eng.* **2003**, *29*, 32.
24. Nilsson, F.; Davidsson, A.; Falas, P.; Bengtsson, S.; Bester, K.; Jonsson, K. Impact of activated sludge ozonation on filamentous bacteria viability and possible added benefits. *Environ. Technol.* **2019**, *40*, 2601–2607. [[CrossRef](#)]
25. Wang, Q.Q.; Gan, J.Y.; Papiernik, S.K.; Yates, S.R. Isomeric effects on thiosulfate transformation and detoxification of 1,3-dichloropropene. *Environ. Toxicol. Chem.* **2001**, *20*, 960–964. [[CrossRef](#)] [[PubMed](#)]
26. Hemdal, J.F. Reduction of Ozone Oxidants in Synthetic Seawater by Use of Sodium Thiosulfate. *Progress. Fish-Cult.* **1992**, *54*, 54–56. [[CrossRef](#)]
27. Pollmann, J.; Ortega, J.; Helmig, D. Analysis of atmospheric sesquiterpenes: Sampling losses and mitigation of ozone interferences. *Environ. Sci. Technol.* **2005**, *39*, 9620–9629. [[CrossRef](#)] [[PubMed](#)]
28. Yang, Y.; Xu, C.; Zhu, Y.; Lin, F.; Ma, Q.; Wang, Z.; Cen, K. Simultaneous removal of SO₂ and NO_x by combination of ozone oxidation and Na₂S₂O₃ solution spray. *CIESC J.* **2016**, *67*, 2041–2047.
29. Yang, J.; Luo, C.; Li, T.; Cao, J.; Dong, W.; Li, J.; Ma, J. Superfast degradation of refractory organic contaminants by ozone activated with thiosulfate: Efficiency and mechanisms. *Water Res.* **2020**, *176*, 115751. [[CrossRef](#)]
30. Ge, L.; Wang, H.; Ma, L.; Li, X. Optimization of extraction process of extracellular substances by physic method. *Environ. Chem.* **2006**, *25*, 722–725.
31. DuBois, M.; Gilles, K.A.; Hamilton, J.K.; Rebers, P.A.; Smith, F. Colorimetric Method for Determination of Sugars and Related Substances. *Anal. Chem.* **1956**, *28*, 350–356. [[CrossRef](#)]
32. Frolund, B.; Palmgren, R.; Keiding, K.; Nielsen, P.H. Extraction of extracellular polymers from activated sludge using a cation exchange resin. *Water Res.* **1996**, *30*, 1749–1758. [[CrossRef](#)]
33. Bureau, N.E. *Methods for Monitoring and Analysis of Water and Wastewater*, 4th ed.; China Environmental Science Press: Beijing, China, 2002; ISBN 9787801634009.
34. Zhang, J.; Tian, Y.; Li, N.; Kong, L.C.; Sun, L.; Yu, M.; Zuo, W. Changes of physicochemical properties of sewage sludge during ozonation treatment: Correlation to sludge dewaterability. *Chem. Eng. J.* **2016**, *301*, 238–248. [[CrossRef](#)]
35. Li, H.; Li, T.; He, S.; Zhou, J.; Wang, T.; Zhu, L. Efficient degradation of antibiotics by non-thermal discharge plasma: Highlight the impacts of molecular structures and degradation pathways. *Chem. Eng. J.* **2020**, *395*, 125091. [[CrossRef](#)]
36. Chen, Y.; Chen, H.; Li, J.; Xiao, L. Rapid and efficient activated sludge treatment by electro-Fenton oxidation. *Water Res.* **2019**, *152*, 181–190. [[CrossRef](#)] [[PubMed](#)]
37. Zhen, G.Y.; Wang, J.H.; Lu, X.Q.; Su, L.H.; Zhu, X.F.; Zhou, T.; Zhao, Y.C. Effective gel-like floc matrix destruction and water seepage for enhancing waste activated sludge dewaterability under hybrid microwave-initiated Fe(II)-persulfate oxidation process. *Chemosphere* **2019**, *221*, 141–153. [[CrossRef](#)] [[PubMed](#)]
38. Wu, B.; Ni, B.J.; Horvat, K.; Song, L.; Chai, X.; Dai, X.; Mahajan, D. Occurrence State and Molecular Structure Analysis of Extracellular Proteins with Implications on the Dewaterability of Waste-Activated Sludge. *Environ. Sci. Technol.* **2017**, *51*, 9235–9243. [[CrossRef](#)]
39. You, G.; Wang, P.; Hou, J.; Wang, C.; Xu, Y.; Miao, L.; Lv, B.; Yang, Y.; Liu, Z.; Zhang, F. Insights into the short-term effects of CeO₂ nanoparticles on sludge dewatering and related mechanism. *Water Res.* **2017**, *118*, 93–103. [[CrossRef](#)]
40. Wu, X.; Li, X.; Yang, Q.; Xu, Q.; Tao, Z.; Huang, X.; Wu, Y.; Tao, L.; Pi, Z.; Chen, Z.; et al. Effect of citric acid on extracellular polymeric substances disruption and cell lysis in the waste activated sludge by pH regulation. *Bioresour. Technol.* **2020**, *302*, 122859. [[CrossRef](#)]
41. Peipei, H.; Guanghui, Y.; Liming, S.; Pinjing, H. Effects of protein and polysaccharide distribution in sludge on dewatering performance. *Environ. Sci.* **2008**, *29*, 3457–3461.
42. Niu, M.; Zhang, W.; Wang, D.; Chen, Y.; Chen, R. Correlation of physicochemical properties and sludge dewaterability under chemical conditioning using inorganic coagulants. *Bioresour. Technol.* **2013**, *144*, 337–343. [[CrossRef](#)] [[PubMed](#)]
43. Niu, T.; Zhou, Z.; Ren, W.; Jiang, L.-M.; Li, B.; Wei, H.; Li, J.; Wang, L. Effects of potassium peroxydisulfate on disintegration of waste sludge and properties of extracellular polymeric substances. *Int. Biod. Biodegrad.* **2016**, *106*, 170–177. [[CrossRef](#)]
44. Sheng, G.-P.; Yu, H.-Q.; Li, X.-Y. Extracellular polymeric substances (EPS) of microbial aggregates in biological wastewater treatment systems: A review. *Biotechnol. Adv.* **2010**, *28*, 882–894. [[CrossRef](#)] [[PubMed](#)]
45. Chen, W.; Zhang, A.; Jiang, G.; Li, Q. Transformation and degradation mechanism of landfill leachates in a combined process of SAARB and ozonation. *Waste Manag.* **2019**, *85*, 283–294. [[CrossRef](#)] [[PubMed](#)]

46. Gholikandi, G.B.; Zakizadeh, N.; Masihi, H. Application of peroxymonosulfate-ozone advanced oxidation process for simultaneous waste-activated sludge stabilization and dewatering purposes: A comparative study. *J. Environ. Manag.* **2018**, *206*, 523–531. [[CrossRef](#)]
47. Li, L.X.; Abe, Y.; Nagasawa, Y.; Kudo, R.; Usui, N.; Imai, K.; Mashino, T.; Mochizuki, M.; Miyata, N. An HPLC assay of hydroxyl radicals by the hydroxylation reaction of terephthalic acid. *Biomed. Chrom.* **2004**, *18*, 470–474.
48. Ding, Q.; Wang, J.; Wang, Y. Detection of hydroxyl radicals in MIL-88A photoFenton catalytic system. *Anal. Inst.* **2021**, *4*, 132–138.

Disclaimer/Publisher’s Note: The statements, opinions and data contained in all publications are solely those of the individual author(s) and contributor(s) and not of MDPI and/or the editor(s). MDPI and/or the editor(s) disclaim responsibility for any injury to people or property resulting from any ideas, methods, instructions or products referred to in the content.